Dynamics at an exceptional point in an interacting quantum dot system

William Samuelson

LUND
UNIVERSITY

Bachelor's Thesis

Supervised by Martin Leijnse and Stephanie Matern

Division of Solid State Physics
Lund University
September 3, 2022

Dynamics at an exceptional point in an interacting quantum dot system

Abstract

A fundamental postulate of quantum mechanics is that the Hamiltonian of a closed system is Hermitian. This guarantees real-valued energies and conserved probabilities throughout the evolution of the system. However, for quantum systems where there is dissipation in and out of the system, such as a collection of quantum dots connected to metallic leads, the dynamics is instead generated by a non-Hermitian Liouvillian superoperator. One feature of non-Hermitian operators with particular theoretical and experimental interest recently, is the possibility of exceptional points. These are points in parameter space which causes two or more eigenvalues and their corresponding eigenvectors of the operator to simultaneously coalesce. Exceptional points have been proposed to have several technological applications and successfully increased the sensitivity of sensors. In this thesis, we analyze a system of two quantum dots coupled in parallel to metallic leads and demonstrate the existence of a second order exceptional point in the Liouvillian superoperator. Furthermore, the dynamics at this exceptional point is simulated using a combination of analytical and numerical methods, including simulations of the density operator and the current through the system. We show that the dynamics can be understood in terms of generalized modes and that the system has a unique algebraic decay at the exceptional point. Furthermore, critical decay at the exceptional point is indicated in the current, in accordance with other works on exceptional points in quantum thermal machines.

Contents

1 Introduction **1**

2 Theory **4**
2.1 Transport through quantum dots 4
2.2 The theory of open quantum systems 5
2.2.1 The von Neumann equation and the reduced density operator 5
2.2.2 The Lindblad Master equation 7
2.3 Exceptional points 8
2.3.1 Jordan normal form 8
2.3.2 General solution of ODEs 10

3 Dynamics at EP in the parallel QD **12**
3.1 Model 12
3.2 Spectrum 14
3.3 Dynamics 15

4 Conclusion and outlook **20**

Chapter 1

Introduction

The theory of quantum mechanics developed in the last century has been proved to be extremely successful in describing nature at the small scale. Typical systems treated by quantum mechanics are nuclei, atoms, and other systems which can be assumed to be isolated from the environment. In such systems, the Hamiltonian is postulated to be Hermitian, guaranteeing that energies are real-valued and that the wave function is contained in the system throughout its evolution [1]. However, for many physical setups we cannot assume the system to be isolated and we must consider the dissipation and the crosstalk between the system and its surroundings. One way to handle such open systems is to loosen the requirement of the Hermiticity of the Hamiltonian. The resulting field of non-Hermitian quantum physics has successfully been describing systems in nuclear, atomic and optical physics in recent decades [2]. One property of particular interest in non-Hermitian operators is the possibility of exceptional points (EPs). These correspond to points in parameter space where two or more eigenvalues and their corresponding eigenvectors of the operator simultaneously coalesce [3]. Exceptional points have been proposed to have several useful technological applications in e.g. optics and photonics [4, 5], and along with the optical microring experiments in 2017, EP sensors successfully increased the sensitivity of current and nano-particle detection [6, 7].

A different framework which treats open systems is quantum master equations, where the dynamics of the system is captured by the Liouvillian superoperator [8]. Similarly to the Hamiltonian in non-Hermitian physics, the Liouvillian is non-Hermitian due to the coupling to the environment. This brings the possibility of EPs also in the Liouvillian superoperator [9]. EPs in Liouvillian physics have been of particular theoretical interest recently, and are proposed to have important applications in control and sensing technologies. Two recent examples include Ref. [10], where critical decay towards the steady state in a quantum thermal machine was found at the EP; and Ref. [11] where an EP corresponded to optimal steering toward a target quantum state.

An application of particular interest for quantum master equations and Liouvillian physics is electron transport in systems of quantum dots connected to metallic leads [12]. A quantum dot (QD) is a fabricated semiconductor structure containing a small number of electrons and is typically in the order of 100 nanometres in size [13]. The size of the dot needs to be small in comparison to the thermal wavelength of the electrons, which is why experiments are generally realized at temperatures close to absolute zero [14]. One method of creating this tiny isolation of electrons is to

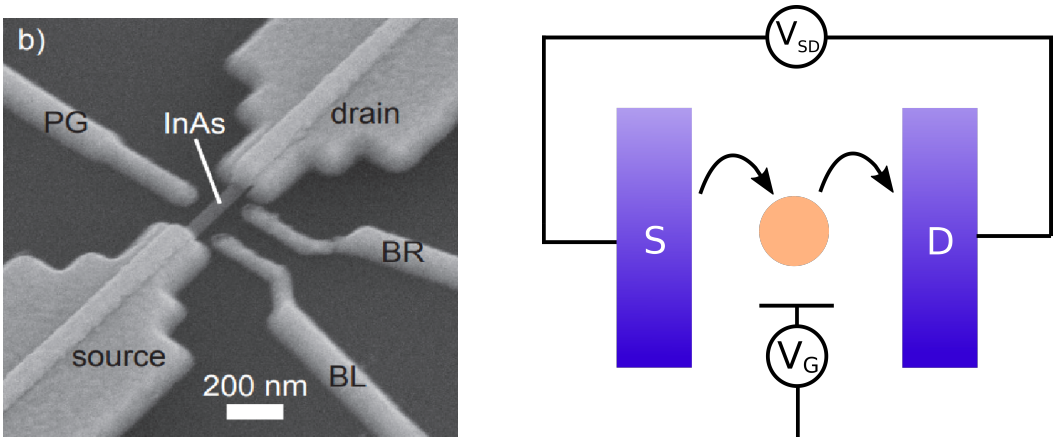

(a) (b)

Figure 1.1: a) A physical implementation of a single QD system. The QD is realized within the InAs nanowire, with the source and drain, and the gates (BR, BL and PG) all clearly visible in this figure. The figure is taken from Ref. [15]. b) A schematic figure of a QD system where the QD is in the center, tunnel coupled to the source (S) and drain (D). The gate voltage V_{G} and the source-drain voltage V_{SD}, are tuned to define the QD.

apply voltages via nanoscale electrodes, called gates, which depletes the number of electrons in a small region, see Fig. 1.1a. If the voltages are tuned successfully, the QD can be tunnel coupled to the two surrounding conducting regions of the semiconductor, known as the source and drain. The electrons can then tunnel from the source into the dot and then exiting it by tunneling into the drain, producing a current through the system [13]. This process is schematically presented in Fig. 1.1b.

The wide tunability of the optical, electrical and chemical properties of QDs has made them useful in a large range of applications. Quantum dot technologies span areas from energy harvesting, display technologies, and sensors to medical and biological applications, with efficient lasers, biotags and solar harvesting devices being available on the market [16]. The transport set-up given in Fig. 1.1 in particular, is used as a very sensitive charge sensor, being able to detect transport of single electron charges, and single electron transistor (source). The QD systems studied in the literature have also included systems containing multiple QDs in various arrangements. In Ref. [17], a system with two QDs coupled in parallel was studied for its quantum interference effects in the transport dynamics, and was proposed to act as a sensitive electric switch.

In this thesis, the parallel QD system was studied for its non-equilibrium transport properties, with focus on the full quantum dynamics, including the transient current. In particular, the dynamics at a second order EP is analyzed in detail using a combination of numerical and analytical approaches. Summarizing the results from the thesis, a second order EP was found, after which we derive and numerically implement the transient dynamics of the parallel dot system at and away from the EP. The evolution of the reduced density matrix in generalized modes is evidenced, including algebraic decay at the EP for certain initial conditions, as opposed to the exponential decay outside of the EP. Furthermore, the simulations of the current through the QDs indicated signatures of critical decay at the EP, similar to the study of quantum thermal machines in Ref. [10].

The thesis is divided in the following sections. In Chapter 2 we present the underlying theory of the thesis, including transport in a QD system, tools used in open quantum systems, and general dynamics at EPs. Chapter 3 consists of three parts. Firstly, a further description of the parallel QD system and the model used for the calculations are given. Then, we construct the Liouvillian and demonstrate the existence of a second order EP. Finally, the dynamics of the density matrix and the current through the system at the EP is simulated. In Chapter 4, we conclude the work and give an outlook on further work and open questions relevant to the field of EPs in Liouvillian physics.

Chapter 2

Theory

The theory chapter of the thesis is divided into three sections. Firstly, a brief overview of the theory behind transport through quantum dots is given. Then, the focus is turned to some of the tools used in open quantum systems, ultimately ending in a section about quantum master equations. The final section will further explain the notion of exceptional points, and introduce important tools used in exceptional point physics. Throughout the following parts of the thesis, we will set the reduced Planck's constant, Boltzmann's constant and the elementary charge to unity, i.e., $\hbar = 1$, $k_b = 1$, and $|e| = 1$.

2.1 Transport through quantum dots

To understand the transport of electrons through a system of quantum dots, it is insightful to first study the single quantum dot system. The following explanation is inspired by Ref. [14].

Consider a single quantum dot with N electrons capacitively coupled to a gate and coupled to source and drain reservoirs through tunnel junctions as in Fig. 1.1b. The main transport properties of the system can then be understood in terms of the chemical potentials of the quantum dot and the source and drain reservoirs. These are often depicted in electro-chemical potential diagrams, see Fig. 2.1. There, $\mu(N)$ is the energy required to add the Nth electron to the quantum dot, and μ_S and μ_D are the Fermi levels of the source and drain. The shaded areas represent the Fermi-Dirac distributions of the reservoirs.

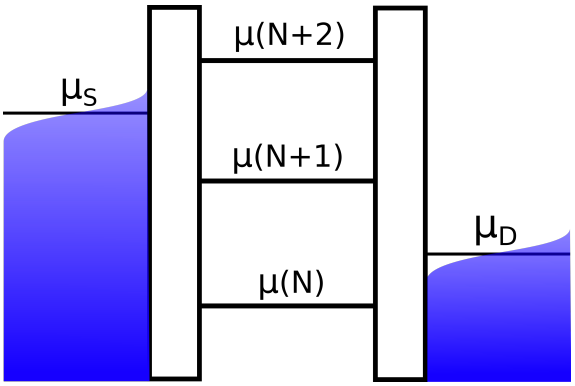

Figure 2.1: An electro-chemical potential diagram of the single quantum dot system. The source and drain are in a thermal distribution given by the shaded areas with Fermi levels μ_S and μ_D. The quantum dot is depicted as a ladder with energies $\mu(N)$, representing the energy required to add the Nth electron to the dot. The figure is adapted from Ref. [14].

Using this picture, the electron transport through the quantum dot can be easily visualized. If the chemical potential levels are located as in Fig. 2.1, $\mu(N+1)$ is below μ_S, and an electron will likely tunnel from the source onto the dot, increasing the number of electrons on the dot from N to $N+1$. After the tunneling event, there is an even lower chemical potential available for the electron, μ_D, and the electron will with a high probability leave the quantum dot and enter the drain. In this fashion, the system will cycle through having N and $N+1$ electrons on the dot, producing a current.

It turns out that $\mu(N)$ depends linearly on the gate voltage V_G, so by changing it, the ladder of states in Fig. 2.1 can be lowered or raised. The source-drain voltage V_{SD} on the other hand, changes the distance between μ_S and μ_D. Through these two processes, it is possible to change the electro-chemical potential landscape and therefore control the current through the system. This captures the main behavior of the dynamics of the quantum dot system. However, by adapting the theory of open quantum systems, a much richer and more accurate theory can be developed.

2.2 The theory of open quantum systems

Open quantum systems are systems which are non-isolated and connected to some sort of environment. Often, it considers a total system consisting of the (sub)system of interest, and an environment. The total system is closed, and therefore it obeys the standard quantum mechanical equations of motion. The goal of the theory of open quantum systems is to infer the dynamics of the smaller system from the equations of the total system [18]. To do this, a few fundamental tools used in this field need to be introduced.

2.2.1 The von Neumann equation and the reduced density operator

An essential tool used in the theory of open quantum systems is the density operator $\hat{\rho}$. In such systems, the exact state of the system is generally unknown. Instead, the

system may be known to be in a state $|\psi_k\rangle$ with a probability p_k, or in another state $|\psi_l\rangle$ with a different probability p_l. Generally, the system is then said to be in an ensemble $\{|\psi_k\rangle, p_k\}_k$. The density operator describes this information in a compact way:

$$\hat{\rho} = \sum_k p_k |\psi_k\rangle \langle\psi_k| . \tag{2.1}$$

It can easily be shown that the density operator is Hermitian and has unity trace, since the probabilities must add up to one. Furthermore, by fixing a basis $\{|\phi_i\rangle\}$, the density operator can be represented by its matrix elements

$$\rho_{ij} = \langle\phi_i|\hat{\rho}|\phi_j\rangle = \sum_k p_k \langle\phi_i|\psi_k\rangle \langle\psi_k|\phi_j\rangle . \tag{2.2}$$

The diagonal elements ρ_{ii} represents classical probabilities of being in a state $|\phi_i\rangle$ and the off-diagonal elements ρ_{ij} are the so called coherences between state $|\phi_i\rangle$ and $|\phi_j\rangle$. Note that the matrix elements are basis dependent, and that there always is a basis in which the density operator is diagonal [8].

The average measured value of an observable $\hat{O}$ of an ensemble represented by $\hat{\rho}$ is given by

$$\langle\hat{O}\rangle = \mathrm{Tr}(\hat{\rho}\hat{O}). \tag{2.3}$$

From the density operator one can therefore extract all signifiant information from the ensemble, and it can be described as the "state" of the system. It is also possible to calculate how the density operator evolves over time. Under a Hamiltonian $\hat{H}$, the evolution is given by the von Neumann equation

$$\frac{\mathrm{d}\hat{\rho}}{\mathrm{d}t} = i[\hat{\rho}, \hat{H}] \equiv \mathcal{L}\hat{\rho}, \tag{2.4}$$

where $\mathcal{L}$ is the Liouvillian superoperator, or just the Liouvillian [8].

The Liouvillian $\mathcal{L}$ in Eq. (2.4) is an operator acting on an operator, hence being called a superoperator. It is however possible represent the Liouvillian as a matrix L, which acts on a vector representation of the density matrices, usually written as $|\rho\rangle\rangle$. The Hilbert space spanned by these vectors is called the Fock-Liouville space, equipped with a scalar product $\langle\langle\rho_1|\rho_2\rangle\rangle$ [18].

Returning to the mentioned goal of the theory of open quantum systems, a natural question is the following: How do we extract the density operator of a subsystem $\hat{\rho}_S$, from the total density operator $\hat{\rho}_T$, the latter describing the closed, full system? This question is resolved by the reduced density operator. If the total system T consists of a subsystem S and an environment E, then the reduced density matrix for the subsystem is given by

$$\hat{\rho}_S = \mathrm{Tr}_E(\hat{\rho}_T), \tag{2.5}$$

where Tr_E is the partial trace over the environment. The partial trace essentially takes the average with respect to the environmental degrees of freedom. This way, a density operator for the subsystem of interest is obtained without having to simulate the whole system. The reduced density operator contains all measurement statistics of interest in the subsystem, placing it at the core of the theory of open quantum systems [8].

2.2.2 The Lindblad Master equation

An important framework for determining the dynamics of an open quantum system is the master equation approach. A classical master equation is defined by

$$\frac{\mathrm{d}p_i}{\mathrm{d}t} = \sum_j R_{ji} p_j - \sum_j R_{ij} p_i, \tag{2.6}$$

with probabilities p_i of being in state $|\psi_i\rangle$, and transition rates R_{ij} describing the rate of transitions from $|\psi_i\rangle$ to $|\psi_j\rangle$. As an example, the states in a quantum dot system may correspond to the number of electrons on the dot while the transition rates are typically related to the Fermi-Dirac distributions of the reservoirs and the tunneling rates of the barriers [14].

Collecting the rate equations for each i and adding the condition $\sum_i p_i = 1$ such that the total probability is unity, a system of ordinary differential equations is obtained. This can be solved numerically using standard methods for first order differential equations, such as the Runge-Kutta method [19]. Once the probabilities $p_i(t)$ are obtained, the evolution of the system can be calculated. Returning to the quantum dot example, the transient dynamics of the current can then be calculated by considering the amount of charge tunneling through the barriers at each point in time, which is directly related to the tunneling rates and probabilities $p_i(t)$ [14].

While a classical master equation may give accurate results for some quantum systems, it leaves out important physics. A quantum master equation generalizes the notion of a classical master equation in the following sense: The unknown in a quantum master equation does not only contain the probabilities p_i of being in a quantum state $|\psi_i\rangle$, but also the coherences. Hence, a quantum master equation involves the full density matrix while a classical master equation only includes the diagonal elements. As discussed previously, it is always possible to find a diagonal density matrix, however this might be in a basis consisting of superposed states, which the classical master equation cannot capture.

The starting point for quantum master equations is Eq. (2.4), the von Neumann equation, for the density matrix of the total system. Using the partial trace, a differential equation for the reduced density matrix of the system of interest (from now on written as $\hat{\rho}$) can be obtained. However, the resulting equation still includes the total density operator and approximations have to be made [18]. One common approximation is to assume that the coupling between the system and the environment is weak in comparison to the other energy scales of the system. This way, the interaction can be treated perturbatively. One of the most established quantum master equations, the Lindblad equation, is derived in this fashion [20], and is given by

$$\frac{\mathrm{d}\hat{\rho}}{\mathrm{d}t} = i[\hat{\rho}, \hat{H}_{\mathrm{eff}}] + \sum_i \hat{J}_i \hat{\rho} \hat{H}_i^\dagger - \frac{1}{2}\hat{\rho}\hat{J}_i^\dagger \hat{J}_i - \frac{1}{2}\hat{J}_i^\dagger \hat{J}_i \hat{\rho} \equiv \mathcal{L}\hat{\rho}, \tag{2.7}$$

where $\hat{H}_{\mathrm{eff}}$ is the sum of two terms: the subsystem Hamiltonian $\hat{H}_{\mathrm{S}}$ and the Lamb shift Hamiltonian $\hat{H}_{\mathrm{LS}}$, a renormalization of energy levels due to the interaction with the environment [18]. The operators $\hat{J}_i$ are the so called jump operators, which capture the coupling processes to the environment. In Ref. [21], a phenomenological approach for calculating the jump operators is described. Using this so called PER-Lind approach, each jump operator is associated with an actual, physical process. Taking a quantum dot system as an example, every jump operator then represents

a certain tunneling event. Once the jump operators are constructed and the first term of Eq. (2.7) is calculated, an expression for the Liouvillian $\mathcal{L}$ can be obtained.

The right hand side of the Lindblad equation can be divided into two parts. The first term, $i[\hat{\rho}, \hat{H}_{\text{eff}}]$, describes the unitary, free evolution of the system. A simple example of a free evolution would be the precession of magnetic moment in a magnetic field. The sum over i on the other hand, labeling, e.g., different tunneling events, correspond to the non-unitary and dissipative part of the dynamics [8]. The latter part causes the total Liouvillian to be non-Hermitian, which brings the possibility of exceptional points in the matrix representation of the Liouvillian.

2.3 Exceptional points

A matrix which describes the evolution of a physical system, such as a Hamiltonian or a Liouvillian matrix, generally depends on the parameters of the system. These parameters span the so called parameter space, and it is in this space the exceptional points lie. An exceptional point is defined as a point in the parameter space which causes two or more eigenvalues and their eigenvectors to simultaneously coalesce [2]. An EP is said to be of a certain order, reflecting how many eigenvectors coalesce at the point. The notion of exceptional points and its orders are directly related to a type of matrix decomposition, the Jordan normal form.

2.3.1 Jordan normal form

In physics, a common way to simplify calculations is to diagonalize the matrix generating the evolution of the system. The diagonalization process can be understood a change of basis to linearly independent eigenvectors r_i, such that $Ar_i = \lambda_i r_i$, where λ_i is the corresponding eigenvalue [22]. In this basis, the linear transformation of the matrix is very simple: it scales each eigenvector r_i by the corresponding eigenvalue. The matrix in the new basis is therefore diagonal, explaining the name of the process. For a matrix A and its diagonal form D, this can be written as

$$A = SDS^{-1}, \tag{2.8}$$

where $S = (r_1, \ldots, r_n)$ consists of the eigenvectors of A.

However, not all matrices can be diagonalized, the exceptions being called defective matrices. For a defective matrix, there does not exist a complete basis of eigenvectors, and the diagonalization process is not possible [22]. This is closely related to the notion of exceptional points, since when two eigenvectors coalesce, one dimension is lost and the eigenvectors do not form a basis anymore. A matrix at an EP is therefore always defective.

Fortunately, there is a notion of an "almost diagonal" form for defective matrices, called the Jordan normal form. Recall that in the diagonalizable case, the basis is changed to the linearly independent eigenvectors. To construct the Jordan form for a defective matrix, this basis has to be completed in some way to span the full space. This can be done using Jordan chains [22], which for each eigenvector r_i with

eigenvalue λ_i, consist of vectors $r_i, r_i^{(2)}, \ldots, r_i^{(n_i)}$ defined by

$$\begin{aligned}(A-\lambda_i I)r_i &= 0,\\ (A-\lambda_i I)r_i^{(2)} &= r_i,\\ (A-\lambda_i I)r_i^{(3)} &= r_i^{(2)},\\ &\vdots\\ (A-\lambda_i I)r_i^{(n_i)} &= r_i^{(n_i-1)},\end{aligned} \tag{2.9}$$

where I is the identity matrix. The length of the ith chain, n_i, depends the number of coalescing eigenvectors, and is therefore the same as the order of the corresponding EP. Note that for eigenvectors not involved in an EP, i.e., for eigenvectors which have not coalesced, the Jordan chain is of length one, only consisting of the eigenvectors themselves.

The vectors forming the Jordan chain are also known as the right generalized eigenvectors, which indicates the notion of *left* generalized eigenvectors. Regular left eigenvectors l_i are row vectors, defined by $l_i A = \lambda_i A$. These can then be extended to left generalized eigenvectors in a similar way as the right ones, forming Jordan chains $l_i, l_i^{(2)}, \ldots, l_i^{(n_i)}$. The left generalized eigenvectors can be constructed such that $l_i^{(s)} r_j^{(t)} = \delta_{ij}\delta_{st}$, i.e, biorthogonally to the right generalized eigenvectors [2]. Creating these left and right Jordan chains for each linearly independent eigenvector results in q pairs of chains, each of which are collected into the matrices

$$\begin{aligned}&\{\boldsymbol{r}_i\}_{i=1}^{q}, \text{ where } \boldsymbol{r}_i = \begin{bmatrix} r_i & r_i^{(2)} & \ldots & r_i^{(n_i)}\end{bmatrix},\\ &\{\boldsymbol{l}_i\}_{i=1}^{q}, \text{ where } \boldsymbol{l}_i = \begin{bmatrix} l_i \\ l_i^{(2)} \\ \ldots \\ l_i^{(n_i)}\end{bmatrix}\end{aligned} \tag{2.10}$$

.

Here, the bold font in $\boldsymbol{r}_i$ ($\boldsymbol{l}_i$) indicates a collection of column (row) vectors next to (below) each other, forming a matrix. The set of right generalized eigenvectors from all Jordan chains is called the canonical basis of the transformation. Using this new basis, the transformation matrix M can be formed:

$$M = \begin{bmatrix}\boldsymbol{r}_1 \ldots \boldsymbol{r}_q\end{bmatrix}, \tag{2.11}$$

which also is known as the modal matrix. The inverse modal matrix M^{-1}, can be formed in terms of the left generalized eigenvectors:

$$M^{-1} = \begin{bmatrix}\boldsymbol{l}_1 \\ \vdots \\ \boldsymbol{l}_q\end{bmatrix}, \tag{2.12}$$

since $\boldsymbol{l}_j \boldsymbol{r}_i = \delta_{ij} I$ where I is the $n_j \times n_i$ identity matrix. This follows from the biorthogonality of the left and right generalized eigenvectors.

The Jordan normal form of A is then finally obtained by forming $J = M^{-1}AM$ and has the following structure:

$$J = \begin{bmatrix} J_{n_1}(\lambda_1) & \dots & 0 \\ \vdots & \ddots & \vdots \\ 0 & \dots & J_{n_q}(\lambda_q) \end{bmatrix}, \text{ where } J_{n_i}(\lambda_i) = \begin{bmatrix} \lambda_i & 1 & \dots & 0 \\ \vdots & \ddots & \ddots & \vdots \\ & & \ddots & 1 \\ 0 & \dots & \dots & \lambda_i \end{bmatrix}. \tag{2.13}$$

The Jordan form hence consists of q Jordan blocks $J_{n_i}(\lambda_i)$ on the diagonal, where each block is of size n_i and consists of its eigenvalue on the diagonal and ones on the super diagonal [22]. Note that if all blocks are of size one, i.e., there are no exceptional points, the Jordan form is diagonal. The Jordan normal form can therefore be thought of a generalization of the diagonal form D.

Unfortunately, the Jordan form of a matrix is notoriously difficult to calculate numerically. This stems from the fact that an arbitrary small perturbation away from an EP completely changes the Jordan form. The process is therefore inherently numerically unstable [23]. For simple cases, it is however possible to work around this difficulty by introducing a small tolerance to determine if eigenvalues and their eigenvectors have coalesced. One can then infer the block structure of the Jordan form and construct it manually.

To be able to use the Jordan form in calculations, a substitution $A \to MJM^{-1}$ has to be made, and hence, the matrices M and M^{-1} are also desirable to compute numerically. These matrices consist of the right and left generalized eigenvectors, which can be calculated by the following process. Firstly, the regular eigenvectors are calculated by some numerical method, e.g., the `scipy.linalg.eig` function in Python. If there are coalesced eigenvectors (within the tolerance), the corresponding Jordan chains need then to be computed. This can be done by solving the defining equations for the generalized eigenvectors given by Eq. (2.9). However, since $A-\lambda_i I$ is not of full rank, the equations are underdetermined, meaning that there does not exist a unique solution. A standard way of solving this problem is by using the Moore-Penrose pseudoinverse, which finds one of the solutions to the equation [22]. This process is then repeated until the full Jordan chains for each set of coalescing eigenvectors are calculated, obtaining all of the generalized eigenvectors. Finally, by biorthogonalizing the two sets of vectors, the modal matrix M and its inverse M^{-1} are obtained. Alternatively, M^{-1} can be calculated by numerically inverting M.

2.3.2 General solution of ODEs

A useful application of the Jordan form is for analytical solutions of ordinary differential equations (ODEs). An ODE is a linear differential equation of the form

$$\frac{\mathrm{d}x}{\mathrm{d}t} = Ax. \tag{2.14}$$

Often, the unknown x is a vector, and A a matrix. The solution can then be written as a matrix exponential in the following way:

$$x(t) = e^{At}x(0), \text{ where } e^{At} = \sum_{k=0}^{\infty} \frac{(At)^k}{k!}. \tag{2.15}$$

The matrix exponential can be simplified using Jordan decomposition. It can be shown that $e^{At} = Me^{Jt}M^{-1}$ where M is the modal matrix and

$$e^{Jt} = \begin{bmatrix} e^{J_{n_1}(\lambda_1)t} & \dots & 0 \\ \vdots & \ddots & \vdots \\ 0 & \dots & e^{J_{n_q}(\lambda_q)t} \end{bmatrix}, \text{ where } e^{J_{n_i}(\lambda_i)t} = e^{\lambda_i t} \begin{bmatrix} 1 & t & \dots & \frac{t^{n_i-1}}{(n_i-1)!} \\ \vdots & \ddots & \ddots & \vdots \\ \vdots & & \ddots & t \\ 0 & \dots & \dots & 1 \end{bmatrix}. \tag{2.16}$$

The matrix exponential therefore consists of entries with terms of the form $t^k e^{\lambda_i t}$ [22]. Note that if A is diagonalizable, all blocks are of size one and the entries consist of pure exponentials on the diagonal.

Using this result, the solution to Eq. (2.14) can be written as

$$x(t) = Me^{Jt}M^{-1}x(0). \tag{2.17}$$

This can further be decomposed if one considers the generalized modes of the system. A generalized mode in this context is meant as the solution to the ODE, with an initial condition in a linear combination of vectors in *one* of the Jordan chains. It can be shown that the trajectory then never leaves that Jordan chain throughout the whole evolution.

To show this, suppose first that the initial state is in such an initial state, i.e., in a linear combination of vectors in one of the Jordan chains:

$$x(0) = a_1 r_i + a_2 r_i^{(2)} + \cdots + a_{n_i} r_i^{(n_i)} = \boldsymbol{r}_i a, \tag{2.18}$$

where $a = (a_1, \dots a_{n_i})^T$ is a constant vector and $\boldsymbol{r}_i$ is defined in Eq. (2.11). Inserting this into Eq. (2.17), the solution can be written as

$$x(t) = Me^{Jt}M^{-1}x(0) = Me^{Jt} \begin{bmatrix} \boldsymbol{l}_1 \\ \vdots \\ \boldsymbol{l}_q \end{bmatrix} \boldsymbol{r}_i a = \boldsymbol{r}_i e^{J_{n_i}(\lambda_i)t} a. \tag{2.19}$$

Hence, the solution stays in the space spanned by the initial condition throughout the evolution, as earlier proposed. For an arbitrary initial condition, the solution can be written as a sum over these generalized modes:

$$x(t) = \sum_{i=1}^{q} \boldsymbol{r}_i e^{J_{n_i}(\lambda_i)t} \boldsymbol{l}_i x(0), \tag{2.20}$$

and the initial condition therefore decides what modes are included in the dynamics of the system.

Translating this theory into the language of Liouvillian physics, the underlying ODE is given by the Lindblad equation, transformed to Fock-Liouville space

$$\frac{\mathrm{d}\rho(t)}{\mathrm{d}t} = \mathcal{L}\rho(t) \to \frac{\mathrm{d}}{\mathrm{d}t} |\rho(t)\rangle\rangle = L |\rho(t)\rangle\rangle, \tag{2.21}$$

where L is the matrix representation of the Liouvillian and $|\rho(t)\rangle\rangle$ the vectorized density matrix. Using Eq. (2.20), the solution can then be written in terms of the eigenvalues and generalized eigenvectors of L.

Chapter 3

Dynamics at EP in the parallel QD

Equipped with the necessary theory, the dynamics of the parallel QD system can now be simulated. The equation of motion for the system is the Lindblad equation, given by Eq. (2.7), for the reduced density operator of the two quantum dots. In Fock-Liouville space, this is equation given by Eq. (2.21), with a matrix representation of the Liouvillian L. Specifying the values of the parameters of the system, L can be constructed from the jump operators and the effective Hamiltonian in the Lindblad equation. By then searching for coalescing eigenvalues and eigenvectors of L in the parameter space, EPs can be located, at which the dynamics obey Eq. (2.20). Finally, Eq. (2.3) can be used to simulate the transient current through the parallel QD system.

3.1 Model

In this thesis, a particular quantum dot system was studied, consisting of two quantum dots connected to two leads in thermal equilibrium. The quantum dots are assumed to be coupled in parallel to the leads, meaning that the dots are coupled to the same lead on each side. Furthermore, it is assumed that there is no direct tunneling between the dots. However, we consider an interacting system, with a finite contribution from the Coulomb repulsion between the electrons in the case of double occupancy. A sketch of the model is given in Fig. 3.1.

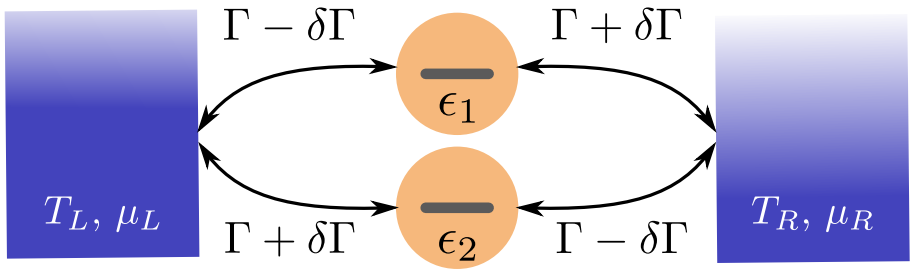

Figure 3.1: The modeled parallel dot system, where the quantum dots in the center have energies ϵ_1 and ϵ_2. Located on the sides are the two reservoirs R, L with temperatures $T_{L/R}$ and chemical potentials $\mu_{L/R}$. The allowed tunneling processes are indicated with arrows, with corresponding tunneling rates $\Gamma \pm \delta\Gamma$.

To reduce the dimension of the parameter space, a fixed tunneling rate Γ and a variable tunneling detuning $\delta\Gamma$ are introduced. The four tunneling rates in terms of

Γ and $\delta\Gamma$ are assumed to be asymmetric, as indicated by Fig. 3.1. It is also assumed that each dot is restricted to be either empty or contain one (spinless) electron in the ground state of the dot. The energy of the ground state $\epsilon_{1/2} = -V_{\mathrm{G}} \pm \delta\epsilon$ is given in terms of a fixed gate voltage $V_{\mathrm{G}} = 0$ and a variable energy detuning $\delta\epsilon$. Furthermore, the temperatures of the leads $T_{\mathrm{L}} = T_{\mathrm{R}} = 10\Gamma$, the chemical potentials $\mu_{\mathrm{L/R}} = \pm V_{\mathrm{SD}}/2$, the bias voltage $V_{\mathrm{SD}} = 300\Gamma$, and the Coulomb energy $U = 250\Gamma$, are all fixed in terms of Γ. This leaves the two tuning parameters, $\delta\Gamma$ and $\delta\epsilon$, as the only parameters of the system, resulting in a two dimensional parameter space.

The total system can be modeled by the Hamiltonian

$$\hat{H} = \hat{H}_{\mathrm{QD}} + \hat{H}_{\mathrm{leads}} + \hat{H}_{\mathrm{tunneling}}, \tag{3.1}$$

where the three terms correspond to the quantum dot, lead, and tunneling Hamiltonians

$$\begin{aligned} \hat{H}_{\mathrm{QD}} &= \sum_{i=1,2} \epsilon_i \hat{d}_i^\dagger \hat{d}_i + U \hat{d}_1^\dagger \hat{d}_1 \hat{d}_2^\dagger \hat{d}_2, \\ \hat{H}_{\mathrm{leads}} &= \sum_{k,s=\mathrm{L,R}} E_{s,k} \hat{c}_{s,k}^\dagger \hat{c}_{s,k}, \\ \hat{H}_{\mathrm{tunneling}} &= \sum_{i=1,2} \sum_{k,s=\mathrm{L,R}} t_{s,i} \hat{c}_{s,k}^\dagger \hat{d}_i + t_{s,i}^* \hat{d}_i^\dagger \hat{c}_{s,k}, \end{aligned} \tag{3.2}$$

where $\hat{d}_i^\dagger$ ($\hat{d}_i$), $i \in \{1,2\}$, creates (annihilates) an electron in dot 1 or 2, and $\hat{c}_{l,k}^\dagger$ ($\hat{c}_{l,k}$), $s \in \{\mathrm{L,R}\}$, creates (annihilates) an electron in the left (L) or right (R) lead with momentum k and energy $E_{s,k}$ [17]. The tunneling amplitudes $t_{s,i}$ are directly related to the corresponding tunneling rates by

$$\Gamma_{s,i} = 2\pi\nu_F |t_{s,i}|^2, \tag{3.3}$$

where ν_F is the density of states in the lead, which is assumed to be independent of energy [21].

To represent the operators in matrix form, the many-body eigenstates of the isolated quantum dot Hamiltonian are used as the basis:

$$\begin{aligned} |a\rangle &= |00\rangle \\ |b\rangle &= |10\rangle = \hat{d}_1^\dagger |00\rangle \\ |c\rangle &= |01\rangle = \hat{d}_2^\dagger |00\rangle \\ |d\rangle &= |11\rangle = \hat{d}_1^\dagger \hat{d}_2^\dagger |00\rangle , \end{aligned} \tag{3.4}$$

where n_1 and n_2 in $|n_1 n_2\rangle$ are the number of electrons in dot first and second quantum dot, respectively. The quantum dot and tunneling Hamiltonians are in this basis given by

$$\begin{aligned} \hat{H}_{\mathrm{QD}} &= \epsilon_1 |b\rangle\langle b| + \epsilon_2 |c\rangle\langle c| + (\epsilon_1 + \epsilon_2 + U) |d\rangle\langle d| \\ \hat{H}_{\mathrm{tunneling}} &= \sum_{k,s=\mathrm{L,R}} \left[t_{s,1}^* (|b\rangle\langle a| + |d\rangle\langle c|) + t_{s,2}^* (|c\rangle\langle a| - |d\rangle\langle b|) \right] \hat{c}_{s,k} + \mathrm{H.c.} \end{aligned} \tag{3.5}$$

In the basis given by Eq. (3.4), the elements of the reduced density matrix can be written as $\rho_{\alpha\beta}$, where $\alpha, \beta \in \{a, b, c, d\}$, with 16 matrix elements. However, the only

non-zero off-diagonal elements are ρ_{bc} and ρ_{cb}, i.e, the elements which corresponds to superpositions the two states with one occupied dot. This is the result of charge being a conserved quantity in the total system (source?). The number of elements in $|\rho\rangle\rangle$ is therefore reduced to 6, which in turn means that the Liouvillian effectively can be represented by a 6×6 matrix. The vectorization of the density matrix can be done in several ways, but in this thesis it is given by

$$\rho = \begin{bmatrix} \rho_{aa} & 0 & 0 & 0 \\ 0 & \rho_{bb} & \rho_{bc} & 0 \\ 0 & \rho_{cb} & \rho_{cc} & 0 \\ 0 & 0 & 0 & \rho_{dd} \end{bmatrix} \rightarrow |\rho\rangle\rangle = \begin{bmatrix} \rho_{aa} \\ \rho_{bb} \\ \rho_{cc} \\ \rho_{dd} \\ \mathrm{Re}\,\rho_{bc} \\ \mathrm{Im}\,\rho_{bc} \end{bmatrix}, \tag{3.6}$$

which is an equivalent representation since the density matrix is Hermitian.

To be able to justify the Lindblad approach for calculating the dynamics of the system, one more major approximation has to be made regarding the coupling between the dots and the leads. We must assume that the strength of the coupling between the system and the environment is weak in comparison with the other energy scales in the system, i.e., $\Gamma \ll T, U$. In this so called weak-coupling limit, the Lindblad equation is a standard approach for investigating the dynamics of a quantum dot system. The time evolution of the reduced density matrix is then determined by Eq. (2.7).

3.2 Spectrum

The first step towards simulating the dynamics of the parallel quantum dot system was to calculate the matrix representation of the Liouvillian. The numerical calculations were done in Python using standard tools from the `numpy` and `scipy` packages. An already implemented PERLind approach was used to calculate the four jump operators $\hat{J}_i$, $i \in \{1, 2, 3, 4\}$, each associated with one of the tunneling processes of the system (should I explain which jump operator corresponds with what tunneling process?). The total Liouvillian could then be constructed and compared with the Python-based QmeQ package [24] as a sanity check. The basis and ordering used for L and $|\rho\rangle\rangle$ is given by Eqs. (3.4) and (3.6). Then, the parameter space was searched for exceptional points by numerically calculating the eigenvalues of L for varying $\delta\epsilon$ and $\delta\Gamma$. A degeneracy of eigenvalues was found at $\lambda_5 = \lambda_6 \approx -0.5\Gamma$, for $\delta\Gamma = 10^{-6}\Gamma$ and $\delta\epsilon \approx 0.3\Gamma$, see Fig. 3.2. The corresponding eigenvectors, $|\rho_5\rangle\rangle$ and $|\rho_6\rangle\rangle$, was found to also coalesce, confirming the existence of an exceptional point. The eigenvalue and the left and right eigenvector corresponding to the EP will be denoted by $\bar{\lambda}$, $\langle\langle\bar{\sigma}|$, and $|\bar{\rho}\rangle\rangle$ respectively.

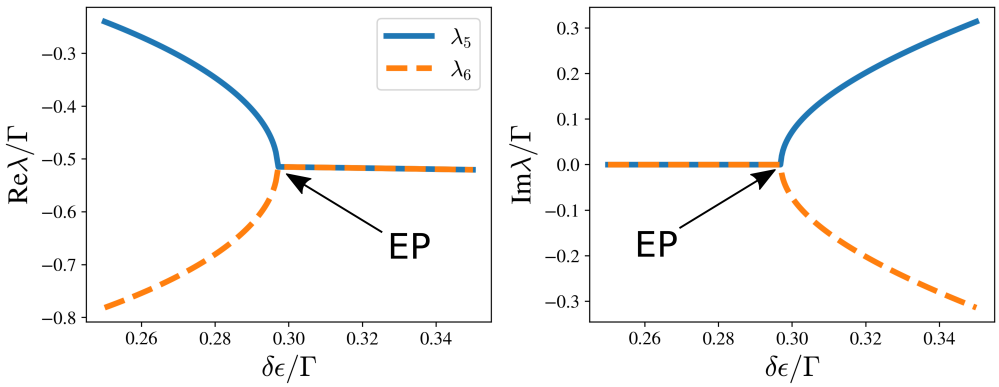

Figure 3.2: The real and imaginary part of two eigenvalues to L, λ_5 and λ_6, for varying $\delta\epsilon$. An eigenvalue degeneracy at can be seen at $\delta\epsilon \approx 0.3\Gamma$.

The full spectrum of the Liouvillian at the exceptional point is given in Fig. 3.3, where the eigenvalue degeneracy between λ_5 and λ_6 is clear. There is almost a degeneracy between λ_3 and λ_4, however, this is not a second EP since the eigenvectors are not parallel. Furthermore, note that all $\lambda_{i>1}$ are on the negative real axis, indicating non-oscillatory, exponential decay towards the steady-state in the dynamics of the system. This steady-state is given by the eigenvector corresponding to the zero eigenvalue λ_1, since then $\frac{\mathrm{d}}{\mathrm{d}t}|\rho\rangle\rangle = 0$.

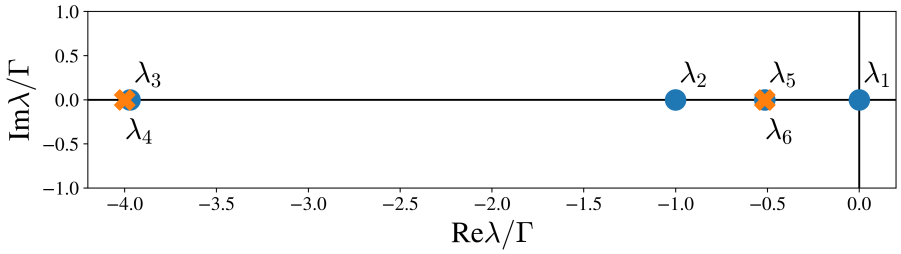

Figure 3.3: The spectrum of the Liouvillian at the EP, where the degeneracy between λ_5 and λ_6 is the relevant one. The crosses are used to distinguish eigenvalues which are close to each other.

3.3 Dynamics

Using Eq. (2.20), the evolution of the system can be given in terms of the eigenvalues and generalized eigenvectors of L. Away from an exceptional point, the Liouvillian is diagonalizable, and the terms are purely exponential. The evolution of the density operator is then given by

$$|\rho(t)\rangle\rangle = |\rho_{ss}\rangle\rangle + \sum_{i=2}^{6} c_i e^{\lambda_i t} |\rho_i\rangle\rangle, \tag{3.7}$$

where $|\rho_i\rangle\rangle$ is the ith right eigenvector of L, and $c_i = \langle\langle\sigma_i|\rho(0)\rangle\rangle$. Here, $\langle\langle\sigma_i|$ is the ith left eigenvector, constructed biorthogonally to $|\rho_i\rangle\rangle$ such that $\langle\langle\sigma_i|\rho_j\rangle\rangle = \delta_{ij}$, and $|\rho_{ss}\rangle\rangle = c_1|\rho_1\rangle\rangle$ is the steady-state of the system. Furthermore, $|\rho_{ss}\rangle\rangle$ is the only

eigenvector with unity trace, which implies that the rest of the other eigenvectors must be traceless for $|\rho\rangle\rangle$ to have unity trace. The eigenvectors $|\rho_{i>1}\rangle\rangle$ do therefore not describe physical states on their own.

At the exceptional point, the Jordan form of L and its exponential $\exp(Jt)$ have to be evaluated. Since the EP is of order two, this results in a 2×2 Jordan block. This is the only EP, which means that rest of the Jordan form is diagonal. Using Eqs. (2.13) and (2.16), this results in the following Jordan form and Jordan exponential:

$$J = \begin{bmatrix} 0 & 0 & 0 & 0 & 0 & 0 \\ 0 & \lambda_2 & 0 & 0 & 0 & 0 \\ 0 & 0 & \lambda_3 & 0 & 0 & 0 \\ 0 & 0 & 0 & \lambda_4 & 0 & 0 \\ 0 & 0 & 0 & 0 & \bar{\lambda} & 1 \\ 0 & 0 & 0 & 0 & 0 & \bar{\lambda} \end{bmatrix}, \; e^{Jt} = \begin{bmatrix} 1 & 0 & 0 & 0 & 0 & 0 \\ 0 & e^{\lambda_2 t} & 0 & 0 & 0 & 0 \\ 0 & 0 & e^{\lambda_3 t} & 0 & 0 & 0 \\ 0 & 0 & 0 & e^{\lambda_4 t} & 0 & 0 \\ 0 & 0 & 0 & 0 & e^{\bar{\lambda} t} & t \\ 0 & 0 & 0 & 0 & 0 & e^{\bar{\lambda} t} \end{bmatrix}, \tag{3.8}$$

since $\lambda_1 = 0$.

Furthermore, the Jordan chain vector, here written as $|\rho'\rangle\rangle$, defined by $(L - \bar{\lambda} I)\,|\rho'\rangle\rangle = |\bar{\rho}\rangle\rangle$ and the corresponding left generalized eigenvector $\langle\langle\sigma'|$ such that $\langle\langle\sigma'|\rho'\rangle\rangle = 1$, need to be evaluated. Inserting these vectors into Eq. (2.20) leads, after a bit of work, to

$$|\rho(t)\rangle\rangle = |\rho_{ss}\rangle\rangle + \sum_{i=2}^{4} c_i e^{\lambda_i t}\,|\rho_i\rangle\rangle + (\bar{c} + c' t) e^{\bar{\lambda} t}\,|\bar{\rho}\rangle\rangle + c' e^{\bar{\lambda} t}\,|\rho'\rangle\rangle, \tag{3.9}$$

where $\bar{c} = \langle\langle\bar{\sigma}|\rho(0)\rangle\rangle$, and $c' = \langle\langle\sigma'|\rho(0)\rangle\rangle$.

By numerically calculating the generalized eigenvectors as described in Section 2.3.1, the dynamics at non-EP and at EP given by Eqs. (3.7) and (3.9), were implemented. The results were then compared with a numerical ODE-solver, see Fig. 3.4.

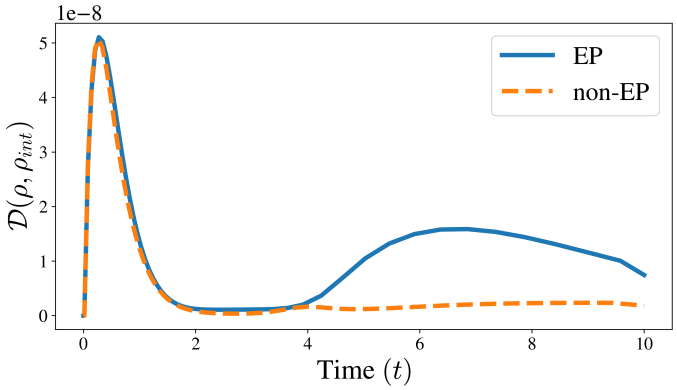

Figure 3.4: The relative difference $\mathcal{D}(\rho, \rho_{\text{int}}) = ||\rho - \rho_{\text{int}}||_1 / ||\rho_{\text{int}}||_1$ between the density matrices calculated with the implemented methods and with a numerical solver. The two lines represent the distances at the EP and away from the EP, using the corresponding implemented methods for each case. The numerical solver was set to an absolute and relative tolerance of 10^{-10} and 10^{-6} respectively.

The relative difference to the numerical solver is on the order of 10^{-8}, and with the use of strict tolerances of the numerical solver, this indicates an accurate method. Furthermore, when reducing the tolerances even more, the distance kept lowering, indicating that the numerical solver might be the limiting factor. It is hence clear that the implemented methods produce an accurate result at and away from the exceptional point.

With a clear picture of the analytical dynamics and numerically calculated eigenvalues and generalized eigenvectors at hand, simulations of the parallel dot system could be done. Firstly, the evolution in the generalized modes was investigated. This was done by introducing initial conditions consisting of linear combinations of the generalized eigenvectors

$$|\rho(0)\rangle\rangle = |\rho_{ss}\rangle\rangle + \sum_{i=2}^{4} b_i \, |\rho_i\rangle\rangle + \bar{b} \, |\bar{\rho}\rangle\rangle + b' \, |\rho'\rangle\rangle. \tag{3.10}$$

This way, the constants c in Eq. (3.9) are the same as the corresponding constants labeled with b in the initial condition. The generalized modes included in the evolution can then be controlled by the initial condition. To see this, simulations of the density matrix were done and then compared with the steady-state of the system, see Fig. 3.5a. The particular initial conditions used for each simulation is given in Table 3.1.

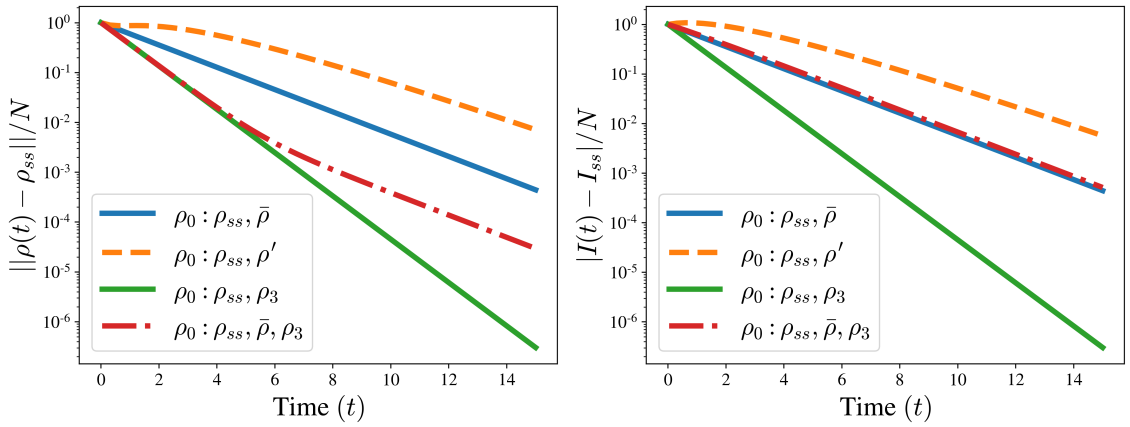

(a) (b)

Figure 3.5: The decay of the density matrix (a) and the current (b), towards the steady-state density matrix ρ_{ss} and current I_{ss} in a logarithmic plot. The simulations were done at the EP with different initial conditions in linear combinations of the generalized eigenvectors given by Table 3.1 and Eq. (3.10). A normalization by $N = ||\rho(0) - \rho_{ss}||$ and $N = ||I(0) - I_{ss}||$ was done such that each curve is unity for $t = 0$.

Table 3.1: The initial conditions used for the simulations in Fig. 3.5, in terms of the constants labeled b in Eq. (3.10). Only the non-zero constants are included in the table.

Line	Constants
Solid, blue	$b = 1$
Dashed, yellow	$b' = 1$
Solid, green	$b_3 = 1$
Dash-dotted, red	$\bar{b} = 1, b_3 = 15$

With initial conditions including only one $b_i \neq 0$ or $\bar{b} \neq 0$, i.e., only one normal eigenvector excluding $|\rho_{ss}\rangle\rangle$, a mode consisting of pure exponential decay toward the steady-state is seen by the straight lines in the logarithmic plot. This is expected since the time evolution only picks up one of the exponentials from Eq. (3.9). The quicker decay corresponds to $|\rho_3\rangle\rangle$ since $|\lambda_3| > |\bar{\lambda}|$, see Fig. 3.3. When including both $|\bar{\rho}\rangle\rangle$ and $|\rho_3\rangle\rangle$ in the initial condition, the decay first follows the quicker decay channel, then gradually turns into following the decay of $|\bar{\rho}\rangle\rangle$. Another behavior is seen for the initial condition including $|\rho'\rangle\rangle$. This generalized mode is not of exponential nature, since a factor of $t\exp(\bar{\lambda}t)$ enters in the dynamics. Away from an EP, the dynamics is given by Eq. (3.7) and this type of algebraic decay never happens. Thus, the behavior of this decay channel is a unique feature of the EP dynamics.

As discussed in the theory section, any relevant observable of the system can be obtained from the density operator. For the parallel dot system, the main observable is the current through the system, which by using Eq. (2.3) can be obtained by

$$\langle \hat{I} \rangle (t) = \mathrm{Tr}\left(\hat{\rho}(t)\hat{I}\right), \tag{3.11}$$

for the current operator $\hat{I}$. The current operator can be phrased in terms of the jump operators $\hat{J}_i$ from the Lindblad equation, which were obtained earlier while calculating the Liouvillian L. By constructing the current operator and implementing Eq. (3.11) numerically, the current through the quantum dot system for varying parameters and initial conditions could be simulated. In Fig. 3.5b, the calculations from Fig. 3.5a were used to also simulate the current for the same initial conditions. The results are similar to the simulations of the density matrix, indicating that the evolution in generalized modes carry over to the transient current dynamics. However, with the initial condition including the two normal eigenvectors, the decay in the quicker decay channel is washed out in this time scale and seemingly only follows the slower decay rate. This can be contrasted with the algebraic decay, which is equally visible in the current dynamics as in the density matrix dynamics.

Simulations were also done to investigate the general behavior of the current at and slightly away from the EP. This is done in Fig. 3.6, for two different initial conditions: one with empty dots, and the other in a mixed state. These initial

density matrices are given by

$$1 : \rho(0) = \rho_{\text{empty}} = \begin{bmatrix} 1 & 0 & 0 & 0 \\ 0 & 0 & 0 & 0 \\ 0 & 0 & 0 & 0 \\ 0 & 0 & 0 & 0 \end{bmatrix}, \tag{3.12}$$

$$2 : \rho(0) = \rho_{\text{mixed}} = 1/4 \begin{bmatrix} 1 & 0 & 0 & 0 \\ 0 & 1 & 0 & 0 \\ 0 & 0 & 1 & 0 \\ 0 & 0 & 0 & 1 \end{bmatrix}.$$

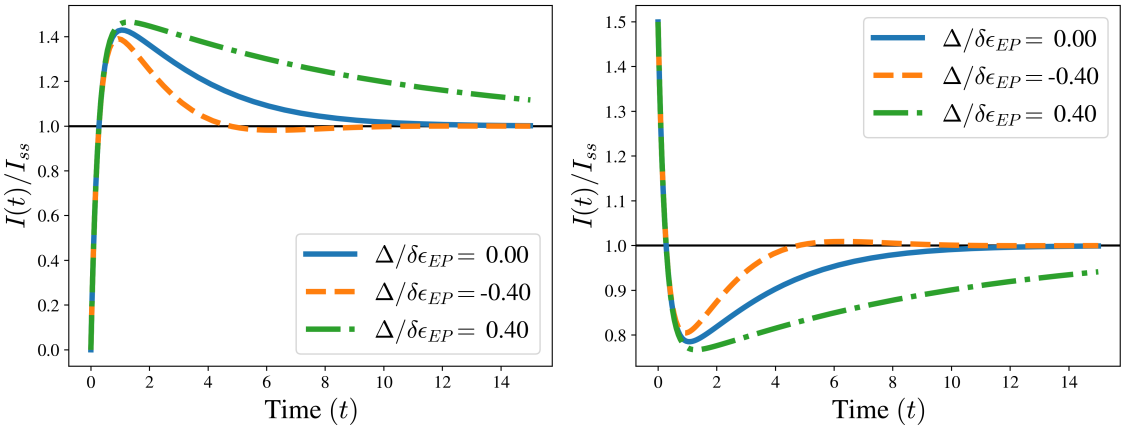

(a) (b)

Figure 3.6: The current over time for different $\Delta = (\delta\epsilon_{\text{EP}} - \delta\epsilon)$, normalized by the corresponding steady-state current I_{ss}. The solid, blue curves correspond to the system being at the EP, while the other two are slightly away from it. The initial conditions are given by Eq. (3.12), with a) having the empty initial condition and b) the mixed one.

Looking at Fig. 3.6, it is clear that the three curves behave differently after the first phase of overshooting the steady-state, i.e., after $t \approx 2$. The curves corresponding to a $\Delta < 0$, slightly overshoot the steady-state once more before approaching the steady-state solution. This can be phrased as an underdamped behavior. On the other hand, for $\Delta > 0$, the decay towards the steady-state is very slow, which can be thought of as an overdamped system. Lastly, for the system at the EP, the decay is much faster than for the overdamped system, but does not overshoot the steady-state again like the underdamped system. This behavior is similar to what was found in Ref. [10] for quantum thermal machines, where it was found that the dynamics at the EP corresponds to the quickest decay without overshooting the steady-state, called critical decay. Furthermore, it can be noted that the current dynamics in Fig. 3.6 varies continuously when approaching and leaving the EP, which is to be expected even though the notion of EPs at first sight seems to invoke abrupt changes. However, there should be no discontinuities in a physical system.

Chapter 4

Conclusion and outlook

In this thesis, we studied the dynamics of a parallel QD system at a second order EP, resulting in both theoretical and computational insights of EP physics for QD systems. To begin with, considering the sparse amount of literature regarding EPs in Liouvillian systems, and in particular systems involving QDs, it is interesting that a system of QDs indeed can give rise to EPs. After finding a second order EP for the parallel dot system, the theory of Jordan decomposition was applied, such that the evolution of the density operator was understood in terms of the generalized modes, given by Eq. (3.9). Intuitively, this means that the Jordan chains, consisting of generalized eigenvectors, evolve separately, and that the initial density matrix decides what modes are involved in the dynamics of the system. Equation (3.9) also implies that the dynamics at the EP for certain initial conditions includes algebraic decay, as opposed to pure exponential decay away from the EP. It was clear that these characteristics of the density operator also carry over to the current through the system. Furthermore, comparisons of the transient current at and away from the EP were done, indicating similarities to Ref. [10] regarding critical decay towards the steady-state at the EP.

From a computational point of view, one may argue that the dynamics could just as well could have been simulated by a standard numerical integrator instead of the implemented methods in this thesis. However, the latter gives direct access to the generalized eigenvectors, which then could be used as initial conditions, directly controlling what modes to be included in the evolution. This increased the understanding of the dynamics of the system and might prove useful for probing the system for interesting and useful dynamics by varying the initial conditions. It is also important to note that the generalized eigenvectors were calculated through numerical means, which in theory can be done for even larger systems and higher order EPs, unlike algebraic methods.

One of the main applications discussed in the literature on EPs is in sensing technologies. This is because eigenvalues are more sensitive to small perturbations at an EP (source). In the framework of non-Hermitian physics, the eigenvalues of the operator in question, the Hamiltonian, are the energies of the system and hence directly observable. In Liouvillian physics, the eigenvalues instead correspond to the decay rates, which are more abstract and difficult to measure. An interesting open problem would be to find a useful observable that probes decay rates, such that similar sensing ideas could be applied to QDs and Liouvillian systems in general. Another proposed application for EPs is in quantum control, i.e., for steering a

quantum state to a target state in an optimal way. This application is perhaps more clear in this thesis since Fig. 3.6 indicates a critical decay toward the steady-state. If a system of QDs would act as a component in a bigger system, it may be important for it to reach the steady state in an optimal way. If so, EPs probably will play a role in this problem.

Bibliography

[1] J. J. Sakurai and J. Napolitano, *Modern quantum mechanics*, 3rd ed. (Cambridge University Press, 2020).

[2] Y. Ashida, Z. Gong, and M. Ueda, "Non-hermitian physics", Advances in Physics **69**, 249–435 (2020).

[3] W. D. Heiss, "Exceptional points of non-hermitian operators", Journal of Physics A: Mathematical and General **37**, 2455–2464 (2004).

[4] M.-A. Miri and A. Alù, "Exceptional points in optics and photonics", Science **363**, eaar7709 (2019).

[5] S. Ozdemir, S. Rotter, F. Nori, and L. Yang, "Parity–time symmetry and exceptional points in photonics", Nature Materials **18**, 1 (2019).

[6] H. Hodaei, A. Hassan, S. Wittek, H. Garcia-Gracia, R. El-Ganainy, D. Christodoulides, and M. Khajavikhan, "Enhanced sensitivity at higher-order exceptional points", Nature **548**, 187–191 (2017).

[7] W. Chen, Ş. Kaya Özdemir, G. Zhao, J. Wiersig, and L. Yang, "Exceptional points enhance sensing in an optical microcavity", Nature **548**, 192–196 (2017).

[8] G. Schaller, *Open quantum systems far from equilibrium*, Vol. 881, Lecture Notes in Physics (2014).

[9] F. Minganti, A. Miranowicz, R. W. Chhajlany, and F. Nori, "Quantum exceptional points of non-hermitian hamiltonians and liouvillians: the effects of quantum jumps", Phys. Rev. A **100**, 062131 (2019).

[10] S. Khandelwal, N. Brunner, and G. Haack, "Signatures of Liouvillian exceptional points in a quantum thermal machine", PRX Quantum **2**, 040346 (2021).

[11] P. Kumar, K. Snizhko, Y. Gefen, and B. Rosenow, "Optimized steering: quantum state engineering and exceptional points", Phys. Rev. A **105**, L010203 (2022).

[12] S. A. Gurvitz and Y. S. Prager, "Microscopic derivation of rate equations for quantum transport", Phys. Rev. B **53**, 15932–15943 (1996).

[13] L. Kouwenhoven and C. Marcus, "Quantum dots", Physics World **11**, 35–40 (1998).

[14] R. A. Bush, E. D. Ochoa, and J. K. Perron, "Transport through quantum dots: An introduction via master equation simulations", American Journal of Physics **89**, 300–306 (2021).

[15] Dorsch, Sven, "Transport in nanowire-based quantum dot systems: Heating electrons and confining holes", eng, PhD thesis (Lund University, 2022).

[16]F. P. G. de Arquer, D. V. Talapin, V. I. Klimov, Y. Arakawa, M. Bayer, and E. H. Sargent, "Semiconductor quantum dots: technological progress and future challenges", Science **373**, eaaz8541 (2021).

[17]Z.-Z. Li and M. Leijnse, "Quantum interference in transport through almost symmetric double quantum dots", Phys. Rev. B **99**, 125406 (2019).

[18]D. Manzano, "A short introduction to the Lindblad master equation", AIP Advances **10**, 025106 (2020).

[19]A. Iserles, *A first course in the numerical analysis of differential equations* (Cambridge University Press, 2009).

[20]G. Lindblad, "On the generators of quantum dynamical semigroups", Communications in Mathematical Physics **48**, 119–130 (1976).

[21]G. Kiršanskas, M. Franckié, and A. Wacker, "Phenomenological position and energy resolving lindblad approach to quantum kinetics", Phys. Rev. B **97**, 035432 (2018).

[22]A. Holst and V. Ufnarovski, *Matrix theory* (Studentlitteratur, 2014).

[23]R. A. Horn and C. R. Johnson, *Matrix analysis* (Cambridge University Press, 1985).

[24]G. Kiršanskas, J. N. Pedersen, O. Karlström, M. Leijnse, and A. Wacker, "QmeQ 1.0: an open-source Python package for calculations of transport through quantum dot devices", Computer Physics Communications **221**, 317–342 (2017).